2023

Geochemical evidence for evolving Proterozoic crustal thickness and orogenic styles in southwestern Laurentia

Ian W. Hillenbrand

Michael L. Williams

et. al.

Recommended Citation
Hillenbrand, Ian W.; Williams, Michael L.; and et. al., "Geochemical evidence for evolving Proterozoic crustal thickness and orogenic styles in southwestern Laurentia" (2023). *Earth and Planetary Science Letters*. 37.
https://doi.org/10.1016/j.epsl.2023.118417

Earth and Planetary Science Letters 622 (2023) 118417

Contents lists available at ScienceDirect

Earth and Planetary Science Letters

journal homepage: www.elsevier.com/locate/epsl

Geochemical evidence for evolving Proterozoic crustal thickness and orogenic styles in southwestern Laurentia

Ian W. Hillenbrand [a,b,*], Karl E. Karlstrom [c], Michael L. Williams [b], Amy Gilmer [a], Wayne Premo [a], Peter Davis [d]

[a] U.S. Geological Survey, Geosciences and Environmental Change Science Center, Denver, CO 80225, USA
[b] Department of Earth, Geographic, and Climate Sciences, University of Massachusetts Amherst, MA 01003, USA
[c] Department of Earth and Planetary Sciences, University of New Mexico, Albuquerque, NM 87106, USA
[d] Department of Geosciences, Pacific Lutheran University, 1010 S 122nd St, Tacoma, WA 98447, USA

ARTICLE INFO

Article history:
Received 20 April 2023
Received in revised form 16 September 2023
Accepted 18 September 2023
Available online 5 October 2023
Editor: A. Webb

Keywords:
Precambrian tectonics
Yavapai orogeny
Picuris orogeny
crustal thickness
magmatic underplate

ABSTRACT

It has long been challenging for researchers to track the crustal thickness and mode(s) of crustal modification in ancient convergent margins, limiting evaluation of the tectonic styles and processes that modify continental crust during orogenesis. We present trace element igneous geochemical crustal thickness proxies that quantitatively track the crustal thickness evolution of the long-lived Proterozoic active margin in the southwestern U.S.A. We integrate these results with geobarometric data to constrain the mode of crustal modification. The data indicate a complex record of crustal thickness change in space and time and evolving orogenic styles. Geochemical proxies at 1.84–1.72 Ga are consistent with 20–40 km thick magmatic arcs that were locally thickened to ~50 km during ~1.75 Ga tectonism. During the Yavapai orogeny, 1.72–1.69 Ga, a ~200-km-wide belt of 50-60 km thick crust extended from southern California to northern Colorado and was rapidly thinned and exhumed by ~1.68 Ga. Crustal thickening and thinning during the Yavapai orogeny largely occurred by shortening and exhumation, respectively, in the upper 25 km of the crust. Subsequent 1.68–1.60 Ga tectonism involved crustal growth, local crustal thickening, and low-P, high-T metamorphism, consistent with extensional accretionary orogenesis. The 1.47–1.37 Ga Picuris orogeny was associated with 50–60 km thick crust across much of the Southwest and involved crustal shortening with ~10 km of magmatic underplating. Advective heat from the emplacement of ferroan granites in the mid-crust likely contributed to elevated geothermal gradients and rheologically weakened the crust. Our results suggest evolving orogenic styles in the Southwest from 1.75–1.69 Ga short-lived crustal thickening associated with terrane accretion to 1.69–1.60 Ga largely extensional accretionary orogenesis, and regional, long-lived crustal thickening at 1.47–1.37 Ga involving extensive basaltic underplating. Contrasting with some recent hypotheses, our data document a complex middle Proterozoic record for the Southwest that was not orogenically quiescent or tectonically stagnant but involved complex mountain building styles.

1. Introduction

Outstanding questions involving mountain building and tectonic processes deep in Earth's past include the height of past mountain belts, extent and duration of thick continental crust, and the nature of processes responsible for changes in crustal thickness (Condie, 1982; Karlstrom and Bowring, 1988; Corrigan et al., 2009; Weller et al., 2021; Roberts et al., 2022). While some workers have hypothesized that orogenic processes since ~2 Ga are largely uniformitarian (Condie, 1982; Corrigan et al., 2009; Weller et al., 2021) others have suggested non-uniformitarian models, particularly for the middle Proterozoic (ca. 1.85–0.85 Ga; Roberts et al., 2022). For example, some workers have suggested that active continental crust in the middle Proterozoic was significantly thinner, and mountain peaks lower, due to either a lack of mountain building events (Tang et al., 2021; Zhu et al., 2022), a single-lid tectonic regime (Stern, 2020), and/or higher geothermal gradients (Spencer et al., 2021).

Quantitative constraints on the crustal evolution of Proterozoic orogens are fundamental for evaluating proposed secular changes in mountain-building processes and the height of past mountain

* Corresponding author.
E-mail address: ihillenbrand@usgs.gov (I.W. Hillenbrand).

https://doi.org/10.1016/j.epsl.2023.118417

belts. Past episodes of crustal thickening have been traditionally inferred from geobarometry and the geometry of metamorphic isograds (Carmichael, 1978; Grambling, 1986; Spear, 1993; Weller et al., 2021). These methods reveal the depth to which rocks exposed at the modern erosional surface were buried but they are not able to resolve the thickness of the entire crustal column (Hillenbrand and Williams, 2021; Weller et al., 2021; Luffi and Ducea, 2022).

We applied whole-rock trace element crustal thickness proxies to a large igneous geochemical dataset to quantify the spatial and temporal evolution of crustal thickness in the Proterozoic orogenic belts exposed in the Southwest U.S.A. The data reveal dramatic spatial and temporal changes associated with orogenic pulses culminating at ca. 1.75, 1.70, 1.65, and 1.40 Ga. The nearly continuous record of crustal evolution from 1.8–1.6 and 1.5–1.3 Ga supports models involving active orogenesis and mountain building in the middle Proterozoic but also highlights changing orogenic styles in this region. These data, along with geophysical imaging, petrologic constraints, and xenolith studies suggest that basaltic underplating may have played a key role in Mesoproterozoic crustal thickening, the generation and emplacement of ferroan granites, and elevated geotherms.

2. Geologic background

Proterozoic rocks exposed in the southwestern U.S.A. are interpreted to have formed along the leading edge of the supercontinent Nuna (Columbia) between 1.8 and 1.3 Ga (Condie, 1982, 2013; Whitmeyer and Karlstrom, 2007; Mitchell et al., 2021). This 1000-km-wide system of orogenic belts has been considered to be a classic example of the growth and stabilization of continental lithosphere through accretionary orogenesis (Condie, 1982, 2013; Karlstrom and Bowring, 1988; Whitmeyer and Karlstrom, 2007). The rocks are interpreted to record multiple tectonothermal events and several crustal provinces have been defined on the basis of geochronologic and isotopic data (Condie, 1982; Bennett and DePaolo, 1987; Karlstrom and Bowring, 1988; Bowring and Karlstrom, 1990; Bickford et al., 2015; Lund et al., 2015) (Fig. 1).

The Mojave Province is composed of ~1.8–1.7 Ga igneous and metasedimentary rocks and is characterized by evolved Nd, Hf, and Pb isotopic signatures (Bennett and DePaolo, 1987; Wooden and Miller, 1990; Holland et al., 2018) (Fig. 1). The Mojave Province may have developed on older, Paleoproterozoic to Archean crustal block(s) or represent a younger arc that incorporated fragments of Archean lithosphere (Wooden and Miller, 1990; Whitmeyer and Karlstrom, 2007; Holland et al., 2018).

The Yavapai Province is made up of 1.8–1.7 Ga igneous and metasedimentary rocks interpreted to represent juvenile crust formed in an arc-related setting (Condie, 1982; Whitmeyer and Karlstrom, 2007; Jones et al., 2011) (Fig. 1). The formation of the Yavapai Province likely involved multiple phases of arc formation and rollback in Colorado and southern Wyoming (Jessup et al., 2005; Jones et al., 2011; Baird et al., 2022). The 1.78–1.76 Ga Green Mountain arc accreted to the margin of the Wyoming craton along the Cheyenne Belt in the 1.76-1.74 Ga Medicine Bow orogeny (Chamberlain, 1998; Jones et al., 2011). Tectono-metamorphism recorded by deformational fabrics and monazite geochronology at generally the same time elsewhere in the Yavapai Province is interpreted to reflect more localized collisions between other arc and/or back-arc terranes outboard of the Wyoming craton (Duebendorfer et al., 2001; Jessup et al., 2005; Hillenbrand et al., 2023). The 1.72–1.69 Ga Yavapai orogeny is interpreted to represent the accretion of the Yavapai and Mojave Provinces to the southern margin of the Laurentian craton (Karlstrom and Bowring, 1988; Bowring and Karlstrom, 1990; Hawkins et al., 1996; Holland et al., 2018) and was contemporaneous with the deposition of 1–2 km thick successions of quartzite and pelite along the southern margin of the Yavapai Province (Jones et al., 2009; Karlstrom et al., 2017; Hillenbrand et al., 2023) (Fig. 1).

The Mazatzal Province lies to the south of the Yavapai Province (Fig. 1) and is interpreted as a continental margin arc that developed on the previously assembled Yavapai Province at 1.7–1.6 Ga (Karlstrom et al., 2016; Holland et al., 2020). Gradational changes in Nd and Pb isotopic data suggest a transitional boundary zone between the Yavapai and Mazatzal Provinces (Shaw and Karlstrom, 1999; Holland et al., 2020). The 1.68–1.60 Ga Mazatzal orogeny involved relatively low grade metamorphism, with high temperatures near syn-tectonic intrusions (e.g. Williams et al., 1999; Duebendorfer et al., 2015). Alternating periods of episodic extension, basin development, and subsequent inversion between 1.68 and 1.60 Ga have been interpreted to reflect changes in the subduction slab-dip angle (Jones et al., 2009; Holland et al., 2020). The period following the Mazatzal orogeny, 1.6–1.5 Ga, was characterized by a lull in magmatism and tectono-metamorphism (Karlstrom et al., 2004). It also included the local deposition of <1.55–1.45 Ga sedimentary successions (Fig. 1) (Doe et al., 2012; Daniel et al., 2013; Jones and Daniel, 2023).

The 1.47–1.37 Ga Picuris orogeny (Daniel et al., 2013) was associated with the widespread emplacement of dominantly ferroan granitic plutons and relatively high temperature, moderate pressure pluton-enhanced regional metamorphism (Williams and Karlstrom, 1996; Williams et al., 1999; Frost et al., 2001; Shaw et al., 2005; Daniel et al., 2023). Regional penetrative deformation, folding, and thrusting associated with the Picuris orogeny occurred in New Mexico and southern Colorado (Shaw et al., 2005; Daniel et al., 2013). Kinematically similar deformation at the same time in Arizona and central to northern Colorado was more localized and included the (re-)activation of shear zones (McCoy et al., 2005; Shaw et al., 2005). Petrogenetic models for the generation of ~1.4 Ga ferroan granites involve mafic underplating, magmatic differentiation, and partial melting of underplated basalts, their differentiated equivalents, and their host rocks in the lower crust (Frost and Frost, 1997, 2023; Frost et al., 2001). Proposed tectonic models include shallow subduction under Laurentia and/or the accretion of the 1.5–1.3 Ga Shawnee Province (Bickford et al., 2015; Holland et al., 2020; Daniel et al., 2023). The Shawnee Province (Lund et al., 2015) lies south of the Mazatzal Province and the isotopically-defined “Nd line” which separates the more isotopically evolved rocks with model ages >1.55 Ga to the north from juvenile rocks with 1.5–1.3 Ga Nd and Hf model ages to the south (Van Schmus et al., 1996; Barnes et al., 1999; Bickford et al., 2015) (Fig. 1).

3. Methods

Correlations between the whole rock geochemistry of igneous rocks, crustal thickness, and surface elevation have been interpreted to reflect the stability and depth-sensitivity of residual minerals such as plagioclase, garnet, and amphibole during magma generation and differentiation near the Moho, as well as the extent of melting (Profeta et al., 2015; Turner and Langmuir, 2015; Luffi and Ducea, 2022 and references therein). The trace element ratios Sr/Y and La/Yb were developed as quantitative paleo-crustal thickness proxies (chemical mohometers) in intermediate composition igneous rocks (55–68 wt% SiO_2; 0–4 wt% MgO, 0.05–0.2 Rb/Sr), albeit with significant uncertainties on the order of 10-15 km (e.g. Profeta et al., 2015). Luffi and Ducea (2022) built on this approach and calibrated 41 “chemical mohometers” involving the abundances and ratios of major and trace elements. These calibrations, based upon a global dataset of ~35,000 samples, account for igneous differentiation using MgO and SiO_2, are applicable to a wider range of mafic and felsic compositions (45–80 wt% SiO_2; 0–10 wt% MgO), and individual mohometers yield a preci-

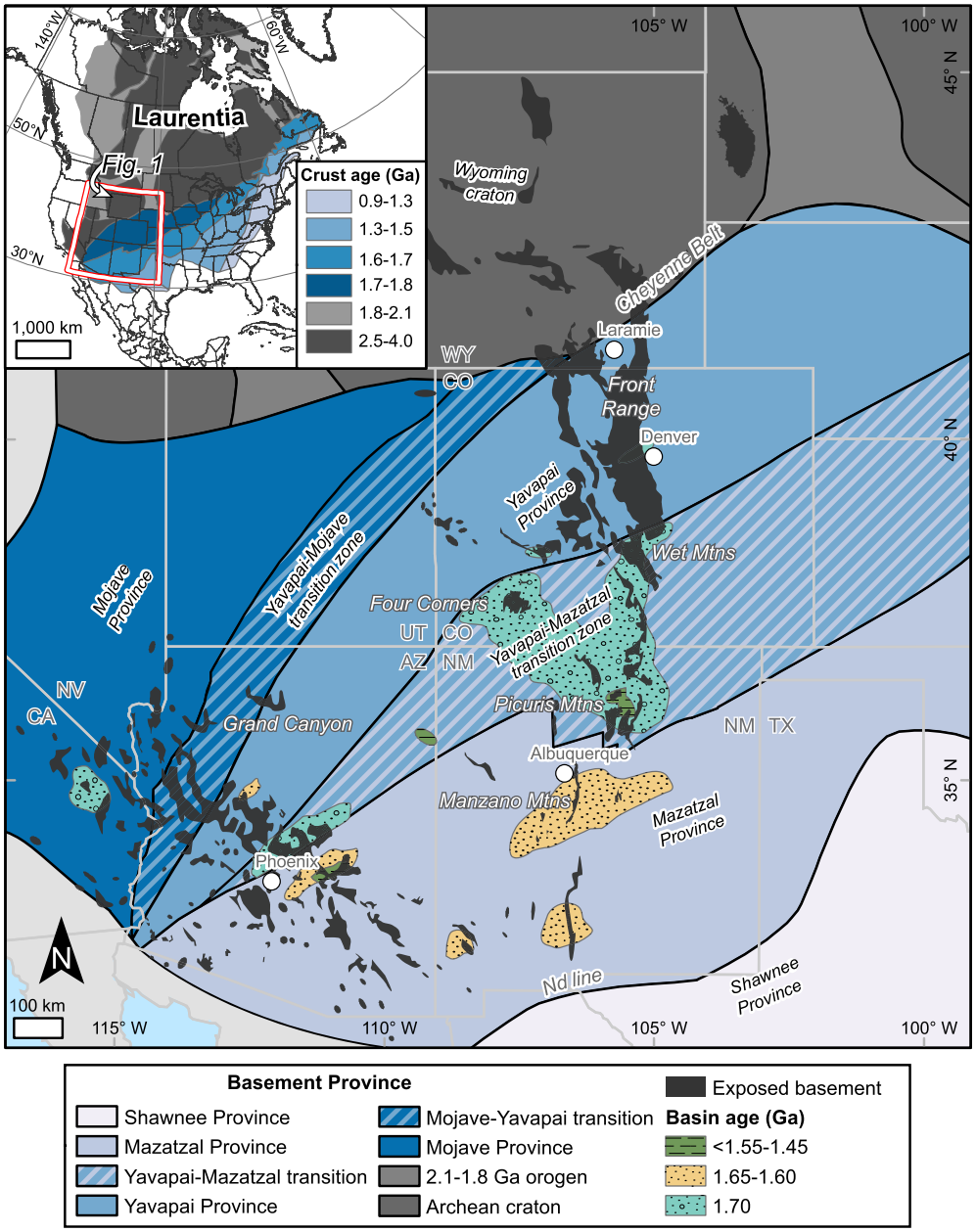

Fig. 1. Simplified geologic map of the Southwest modified from Shaw and Karlstrom (1999), Whitmeyer and Karlstrom (2007), Daniel et al. (2013), Bickford et al. (2015), Holland et al. (2020) and references therein. The age and interpreted extent of Proterozoic basins are from Whitmeyer and Karlstrom (2007), Jones et al. (2009), Jones and Daniel (2023), and Daniel et al. (2013, 2023). AZ – Arizona, CA – California, CO – Colorado, NM – New Mexico, NV – Nevada, TX – Texas, UT – Utah, WY – Wyoming. Mtns – Mountains. Inset: Simplified map of Laurentian crustal age provinces after Whitmeyer and Karlstrom (2007).

sion of ~5 km (Luffi and Ducea, 2022). The application of multiple mohometers (multiproxy chemical mohometry) utilizes the different sensitivity ranges of individual proxies to enhance accuracy and further reduce uncertainties (Luffi and Ducea, 2022). Chemical mohometry paired with geochronologic data offers the ability to reconstruct time resolved records of crustal thickness across the lifespan of convergent margins (Profeta et al., 2015; Hillenbrand and Williams, 2021, 2022).

We applied multiproxy chemical mohometry to a newly compiled geospatial database of igneous whole rock chemical analyses from the Southwest U.S.A. Geochemical data from Proterozoic igneous rocks were compiled from published sources and georeferenced following Hillenbrand and Williams (2021, 2022). Crustal thickness estimates were calculated in the MATLAB-based Geochemical Arc Moho Estimator (GAME) program of Luffi and Ducea (2022). We note that as the calibration of Luffi and Ducea (2022) is based on modern samples, deep time applications require an assumption of similar petrogenetic processes. This assumption has been supported by indication of broadly similar extents of melting and partitioning coefficients since 2.6-2.5 Ga (Keller and Schoene, 2018). We evaluate this assumption for our dataset by comparing multiproxy mohometry with independent geobarometric constraints in Section 5 and discuss this further in section 6.4. Altered samples were removed using the criteria of du Bray et al. (2015): SiO_2 >80 weight %, Na_2O >6.5% or <0.5%, K_2O >10%, CO_2 >0.35%, and/or total volatile concentrations >3% (see also Fig. S1). Individual mohometers with a root mean square error (RMSE) of >3 km were culled as they represent poor fits to the mohometer calibration (Luffi and Ducea, 2022). Outliers were removed using the modified Thompson tau statistical method (Profeta et al., 2015).

Samples with less than three mohometers that yielded an RMSE <3 and/or mohometer standard deviations >10 were eliminated. Filtering reduced the number of samples considered from more than 4,000 to 1,167. Crustal thickness estimates for individual samples were based upon the median of the mohometers that passed the filters (Luffi and Ducea, 2022). The weighted mean and 2σ uncertainty of each unit was calculated from using the median value and standard deviation of individual samples. Data from units were utilized in time series analysis to minimize sampling bias (Turner and Langmuir, 2015; Hillenbrand and Williams, 2021, 2022).

Temporal trends were assessed using a locally estimated scatterplot smoothing (LOESS) running mean with a 30 m.y. moving window. Uncertainty was estimated via bootstrap resampling with replacement 10,000 times (Hillenbrand and Williams, 2022). The moving window interval was selected based upon the precision of available geochronologic dates and sensitivity testing to over and undersmoothing (Hillenbrand and Williams, 2022). Spatial trends in the dataset were evaluated using nearest neighbor interpolation, raster to contour, and raster math tools in ArcMap 10.8 (Kirkland et al., 2011; Hillenbrand et al., 2021; Hillenbrand and Williams, 2021). Nearest neighbor is an interpolation method that finds the closest subset of input samples to a query point and weights them on proportionate areas (Sibson, 1981). This method was utilized because it adapts locally to the structure of the input data, works equally well with regularly and irregularly distributed data, and preserves the values where there are data limiting interpolation artifacts (Sibson, 1981).

4. Results

Crustal thickness estimates were obtained from 1,167 samples from 392 igneous rock units. The samples are largely from the two major Proterozoic outcrop belts in the Southwest, one trending N-S from southern Wyoming to New Mexico and one trending NW-SE from eastern California to southern New Mexico (Fig. 1). Between these belts samples are scarcer and are largely derived from xenoliths and drill core. All data are tabulated in the Supplementary Material (see also Premo et al., 2023). Calculated standard deviations range from 1 to 10 km with a median of 5 km. We present the data as (1) time series organized by crustal province and (2) maps at specific time periods corresponding to regional geologic events, and (3) maps of changes in crustal thickness between time slices. These complementary approaches facilitate investigation of crustal thickness changes across space and time.

4.1. Time series analysis by province

Crustal thickness estimates were calculated for 58 igneous rock units from the Mojave Province and the Mojave-Yavapai transition zone (Fig. 2A). The 1.840 ± 0.001 Ga Elves Chasm gneiss, the oldest exposed rock in the Southwest (Hawkins et al., 1996; Holland et al., 2018), yielded an estimate of 21 ± 3 km (Fig. 2A). The data suggest variations in mean crustal thickness from 30 ± 7 km at ~1.76 Ga to 49 ± 10 km at ~1.75 Ga to 40 ± 6 km at ~1.73 Ga and a peak of 55 ± 6 km at 1.71-1.69 Ga. This was followed by decreases in crustal thickness to 42 ± 6 km at ~1.68 Ga and 38 ± 10 km at ~1.65 Ga (Fig. 2A). Due to the paucity of 1.60–1.50 Ga igneous rocks in the Southwest during the magmatic lull (Karlstrom et al., 2004), we are not able to estimate crustal thickness in this interval. The data suggest mean crustal thicknesses of 48 ± 3 to 50 ± 3 km between 1.45 and 1.37 Ga (Fig. 2A).

Multiproxy chemical mohometry data were obtained from 206 units in the Yavapai Province (Fig. 2B). A decrease in mean crustal thickness is indicated from 35 ± 4 km at ~1.78 Ga to 25 ± 4 km by ~1.72 Ga followed by a sharp increase to 58 ± 5 km at 1.71–1.69 Ga. Subsequently, the data suggest a decrease to 46 ±

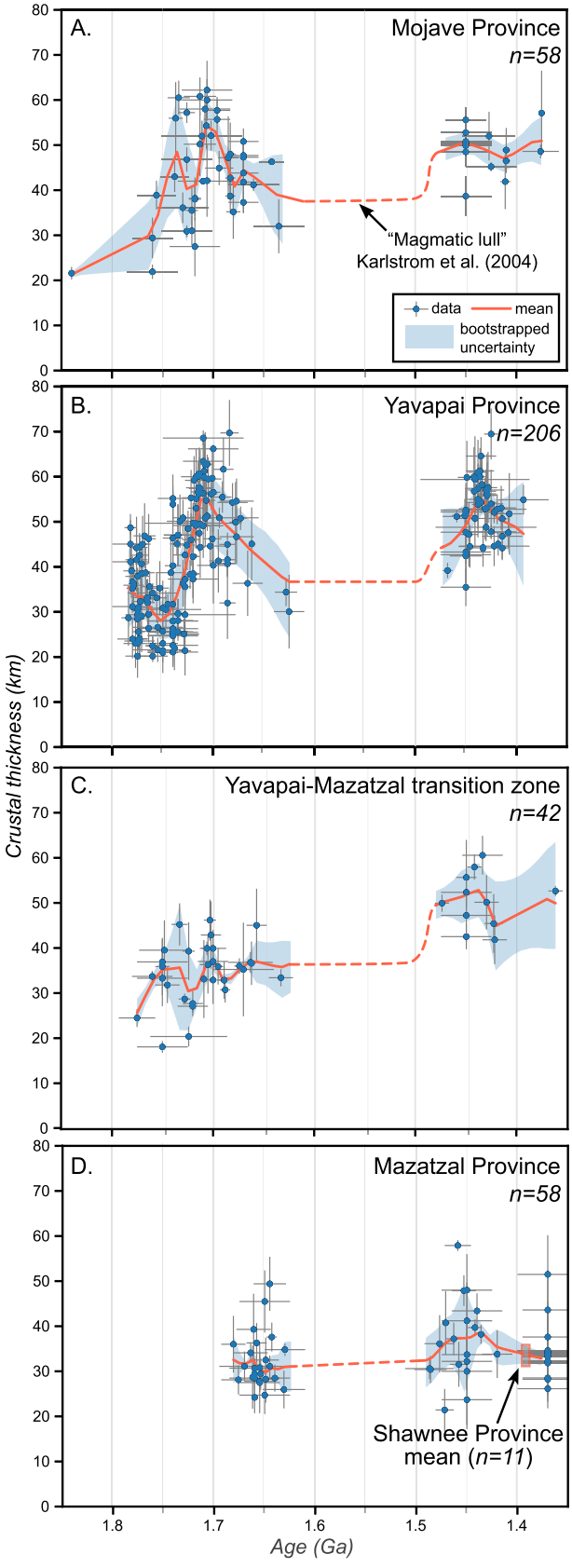

Fig. 2. Crustal thickness time series with LOESS running mean and bootstrapped uncertainty (95% confidence interval) for the Mojave Province and Mojave-Yavapai transition zone (A), Yavapai Province (B), Yavapai-Mazatzal transition zone (C), and Mazatzal Province (D). The path is dashed at 1.6-1.5 Ga due a paucity of data associated with the magmatic gap (Karlstrom et al., 2004). Data points show weighted mean values and 2σ uncertainties for each igneous rock unit.

8 km at ~1.68 Ga and to ~34 km at ~1.63 Ga (Fig. 2B). No data are available in the interval 1.63–1.47 Ga. Mesoproterozoic mean crustal thickness in this province varied from 43 ± 7 km at ~1.47 Ga to 56 ± 4 km at ~1.45 Ga and 50 ± 7 km at ~1.40 Ga (Fig. 2B).

Geochemical data from 42 units in the Yavapai-Mazatzal transition zone were used to constrain crustal thickness between ~1.76 and 1.36 Ga. The proxies suggest a moderately thin crust between ~1.76 and ~1.63 Ga, yielding mean values of 26 ± 5 km at ~1.76 Ga, 34 ± 3 km at ~1.75 Ga, 29 ± 4 km at ~1.71 Ga, and 35 ± 5 km at 1.70-1.63 Ga (Fig. 2C). The data suggest greater mean values of 49 ± 4 km at ~1.47 Ga, 52 ± 5 at ~1.44 Ga, and 44 ± 8 km at ~1.41 Ga (Fig. 2C). The 1.362 ± 0.007 Ga San Isabel Granite (Bickford et al., 2015) yielded a 52 ± 3 km crustal thickness estimate (Fig. 2C).

Crustal thickness estimates from the Mazatzal Province (n=58 units) indicate a mean crustal thickness of 33 ± 3 at ~1.68 Ga with a minor decrease to 29 ± 2 km by ~1.62 Ga (Fig. 2D). The data suggest a mean crustal thickness of 33 ± 6 km at ~1.48 Ga, an increase to 39 ± 8 km at 1.46-1.44 Ga, and a decrease to 32 ± 2 km by ~1.37 Ga.

Crustal thickness estimates from the Shawnee Province (Fig. 2D) gave a mean of 30 ± 3 km at 1.4 Ga (n=11). No time series was constructed due to the limited availability and range of U-Pb dates in this region (Van Schmus et al., 1996; Barnes et al., 1999; Bickford et al., 2015).

4.2. Time slice maps

To further investigate time-space variations in crustal thickness we constructed orogen-scale maps at geologically significant time periods (Kirkland et al., 2011; Mole et al., 2019; Hillenbrand and Williams, 2021). The maps (time slices) in Figs. 3 and 4 were informed by, and designed to investigate, time periods previously reported to correspond to significant geologic events (see section 2; cf., Whitmeyer and Karlstrom, 2007 and references therein). Maps were constructed with nearest neighbor interpolation and incorporate all geochemical data points that passed filters.

Fig. 3 shows geochemical crustal thickness proxies at 1.84–1.76 Ga (Fig. 3A), 1.76–1.74 Ga (Fig. 3B), and 1.74–1.72 Ga (Fig. 3C). The oldest time slice (Fig. 3A) suggests crustal thickness on the order of ~30-40 km in northern Colorado and southern Wyoming and ~25–30 km in central Colorado, northern New Mexico, and Arizona. Chemical mohometric data for 1.76-1.74 Ga (Fig. 3B) indicate 25–35 km crustal thickness estimates in northern New Mexico and Colorado, ~35 km near Four Corners, ~45 km in the Grand Canyon, and ~50–55 km in northwestern Arizona and eastern California. Chemical mohometric constraints from the 1.74-1.72 Ga interval suggest 25–40 km mean values for most of the Mojave and Yavapai Provinces and Yavapai-Mazatzal transition zone (Fig. 3C). The greatest mean estimates (40–50 km) at this time are in northern Colorado and eastern California (Fig. 3C).

Fig. 4A shows geochemically-derived crustal thickness estimates in the 1.72–1.69 Ga age range (i.e. the Yavapai orogeny; Karlstrom and Bowring, 1988). The figure shows a region of ~50–60 km thick crust that extends from California to Grand Canyon and across Four Corners to central and northern Colorado in the Mojave and Yavapai Provinces (Fig. 4A). To the south (present coordinates), the data suggest crustal thicknesses on the order of 30–40 km in the Yavapai-Mazatzal transition zone (Fig. 4A).

Crustal thickness estimates at 1.69–1.60 Ga, the time period generally corresponding with the Mazatzal orogeny (Duebendorfer et al., 2015), range from ~25 km to ~45 km (Fig. 4B). Samples from the Mojave and Yavapai Provinces yielded crustal thickness estimates on the order of ~40–45 km (Fig. 4B). Geochemical

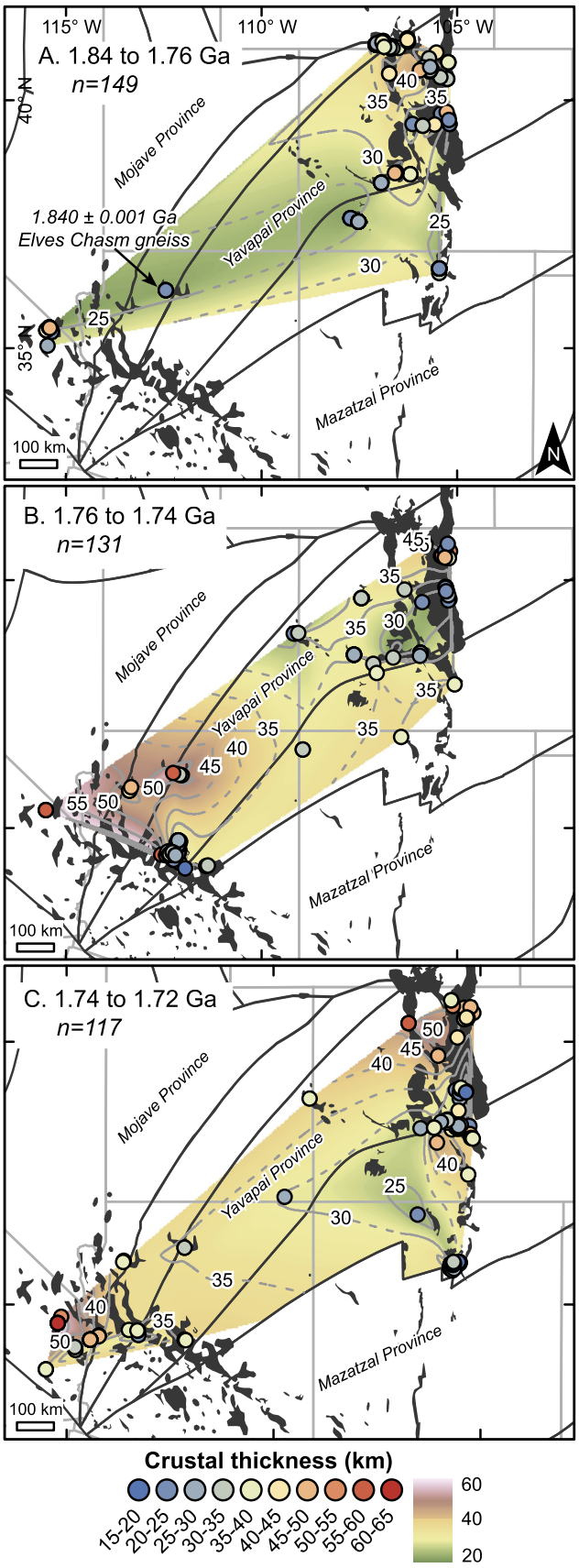

Fig. 3. Time slice maps of crustal thickness at 1.84-1.76 Ga (A), 1.76-1.74 Ga (B), and 1.74-1.72 Ga (C). Present day basement exposures and boundaries of crustal provinces are shown for reference. Note: contour lines are dashed where the dataset is more limited.

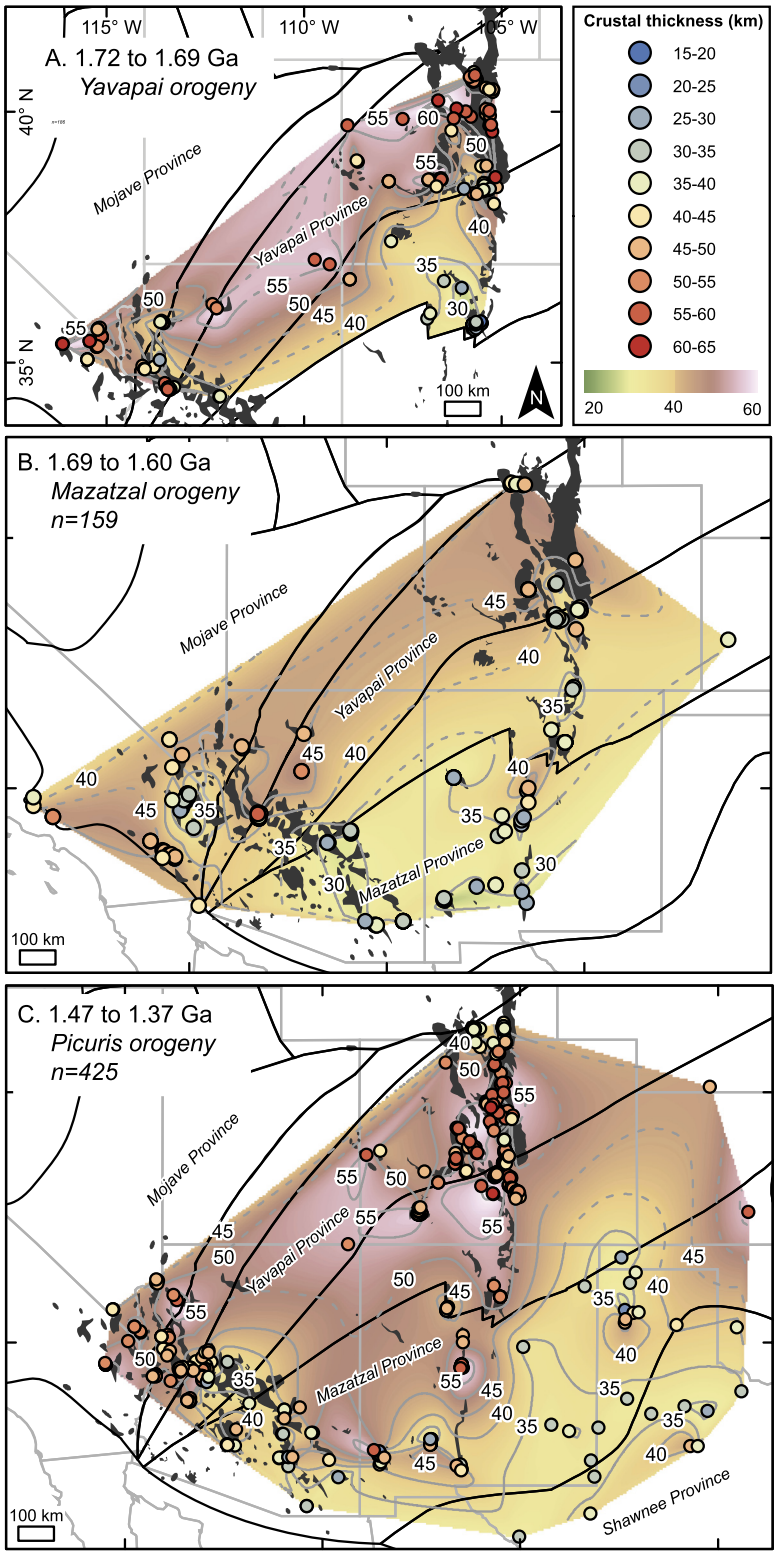

Fig. 4. Time slice maps of crustal thickness during at 1.72-1.69 Ga (A), 1.69-1.60 Ga (B), and 1.47-1.37 Ga (C). Present day basement exposures and boundaries of crustal provinces are shown for reference. Note: contour lines are dashed where the dataset is more limited.

proxy data from the Yavapai-Mazatzal transition zone and Mazatzal Province in southern Arizona, southern Colorado, and New Mexico yielded thinner estimates, on the order of 25–40 km (Fig. 4B).

Samples dated to 1.47–1.37 Ga (i.e. Picuris orogeny; Daniel et al., 2013) indicate a broad region with crustal thickness estimates on the order of 50–60 km from northern Colorado to central New Mexico and eastern California (Fig. 4C). Marginal to this region, in southern Wyoming, central Arizona, southern and eastern New Mexico, and the Shawnee Province, the chemical mohometry suggests thinner crust, on the order of ~30–40 km (Fig. 4C).

4.3. Results of spatial changes in crustal thickness

We calculated the magnitude of crustal thickness changes between time slices with the raster math tool in ArcMap 10.8 (Hillenbrand and Williams, 2021). Comparison of the 1.74–1.72 Ga and 1.72-1.69 Ga time slices (Fig. 5A) suggests 10–25 km of crustal thickening from Grand Canyon through Four Corners to northern Colorado in the Mojave and Yavapai Provinces. This is consistent with the region of ≥50 km thick crust in the same region shown in Fig. 4A. In contrast, between 10 km of crustal thickening and 5 km of crustal thinning are indicated in the Yavapai-Mazatzal transition zone (Fig. 5A).

Fig. 5B shows changes between the 1.72–1.69 Ga and 1.69–1.60 Ga time slices. The map indicates 5-10 km of crustal thinning in a NE-SW trending belt of north of the Yavapai-Mazatzal transition zone in eastern California, Grand Canyon to Four Corners, and central to northern Colorado. The area of thinning corresponds to the region of 50–60 km thick crust at 1.72–1.69 Ga (Fig. 4A). In the Yavapai-Mazatzal transition zone the data indicate relatively minimal changes in crustal thickness and suggest as much as ~5 to 10 km of local crustal thickening in northern New Mexico and western Arizona (Fig. 4B).

Comparison of the 1.69–1.60 Ga and 1.45–1.37 Ga time slices (Fig. 5C) suggests an 5–20 km increase in crustal thickness across much of Colorado, and no resolvable change in crustal thickness in west-central Arizona. The broadest region of 15–20 km crustal thickening is within the Yavapai-Mazatzal transition zone and Mazatzal Province in southern Colorado to central New Mexico (Fig. 5C).

5. Synthesis of geochemical and geobarometric data

Igneous geochemical data from the Southwest provide a nearly 500 m.y. record (1.8–1.3 Ga) of crustal thickness variation. In the following paragraphs, we synthesize the results of this dataset and integrate it with geobarometric data to evaluate the evolution of crustal thickness and orogenesis in the Southwest. As described below, the spatial and temporal resolution of our crustal thickness dataset, when enhanced by the geobarometric data, provides a number of new insights into the record of Proterozoic crustal evolution.

5.1. Synthesis of chemical mohometry

The oldest exposed rocks in the Southwest, ca. 1.84–1.72 Ga, largely yielded crustal thickness estimates on the order of 25–40 km with values of 45–55 km indicated only in localized regions and for short durations (<15 m.y.) (Figs. 2A; 3B-C). Crustal thickening (up to 50–60 km) is recorded at 1.72–1.69 Ga in the Mojave and Yavapai Provinces with thinner crust (25–40 km) in the Yavapai-Mazatzal transition zone (Figs. 2A-B; 4A). This crustal thickening event was also relatively short-lived; data suggest it was followed by ~10-15 km of thinning between ~1.70 and ~1.68 Ga (Figs. 2A-C; 4A-B; 5A). At 1.69–1.60 Ga the data indicate localized crustal thickening on the order of 5-10 km within the Yavapai-Mazatzal transition zone and ~10 km of crustal thinning in the Yavapai and Mojave Provinces (Figs. 2, 5). Finally, 5–20 km crustal thickening to 50-60 km before 1.45 Ga is indicted across much of the Southwest (Fig. 5C).

Taken together, multiproxy chemical mohometry reveals four Proterozoic crustal thickening events in the Southwest at ca. 1.75, 1.72–1.69, 1.68–1.60, and 1.45–1.37 Ga, with those at 1.72–1.69 and 1.45–1.37 Ga being the most significant. These intervals, indicated by whole rock geochemistry, correlate with geologic observations, structural geology, petrologic, and geochronologic evidence for regional orogenic events including the ~1.75 Ga accretion of the

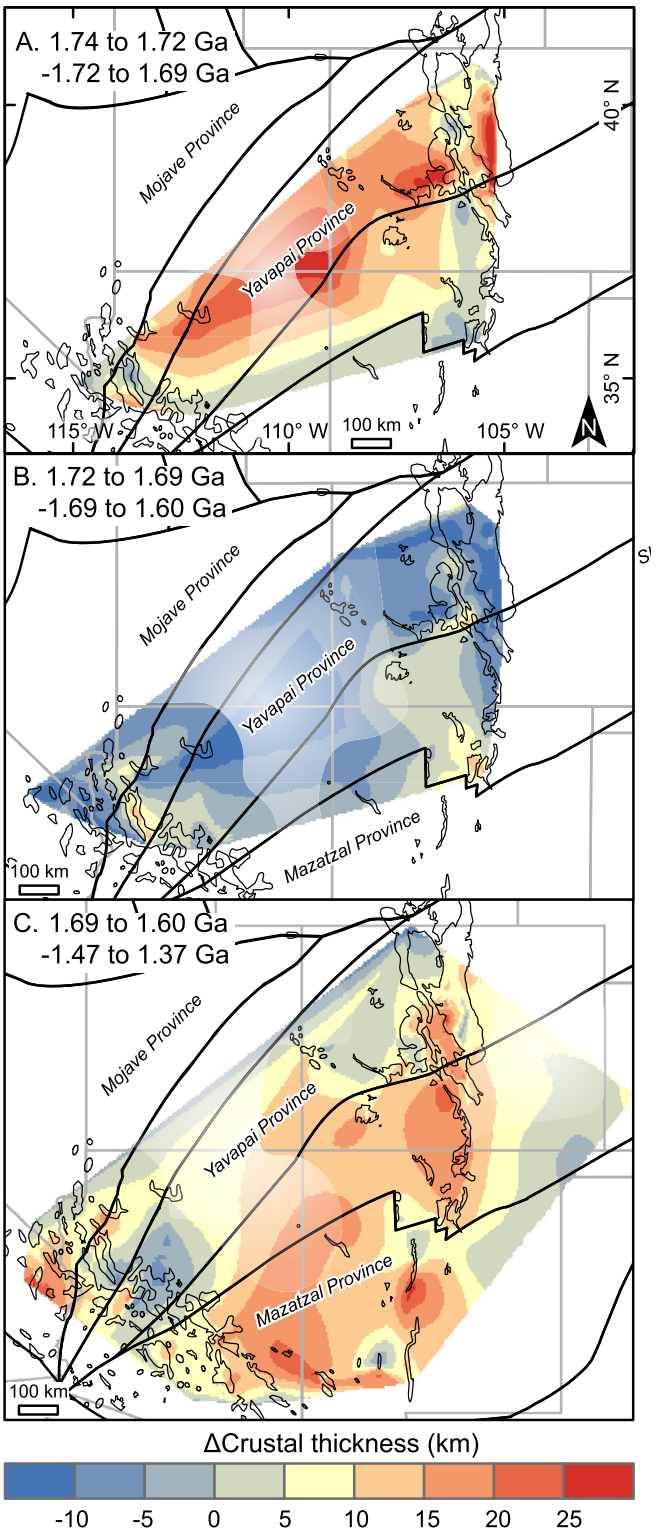

Fig. 5. Maps of change in crust thickness between time slices calculated using ArcGIS raster math. A: Change in crustal thickness between the 1.74-1.72 Ga and 1.72-1.69 Ga time slices involved regional crustal thickening. B: Change in crustal thickness between the 1.72-1.69 Ga and 1.69-1.60 Ga time slices indicating regional crustal thinning in the Yavapai and Mojave Provinces. C: Change in crustal thickness between the 1.69-1.60 Ga and 1.47-1.37 Ga time slices involved renewed crustal thickening over a broad region. Note that the constraints are primarily from basement exposures (shown as outlines) and lesser confidence is placed on in the intervening areas which have fewer constraints. The opacity of the interpolated map is increased in areas where the dataset is more limited.

Mojave and Yavapai Provinces (Duebendorfer et al., 2001; Holland et al., 2018), 1.72–1.69 Ga Yavapai orogeny (Bowring and Karlstrom, 1990; Karlstrom and Bowring, 1988), 1.68–1.60 Ga Mazatzal orogeny (Shaw and Karlstrom, 1999; Duebendorfer et al., 2015; Holland et al., 2020), and 1.47–1.37 Ga Picuris orogeny (Shaw et al., 2005; Daniel et al., 2013, 2023).

5.2. Geobarometric constraints

Many studies have inferred past episodes of crustal thickening on the basis of metamorphic assemblages and geobarometry (e.g. Carmichael, 1978; Grambling, 1986; Spear, 1993; Dumond et al., 2007; Weller et al., 2021). We compiled previously published quantitative geobarometric data from the Southwest (Supplementary Material). This compilation was limited to samples exposed at the modern erosional surface with well constrained ages so that they could be linked with orogenic phases and igneous geochemical crustal thickness proxies. Geobarometric data were converted to burial depth assuming a typical crustal density of 2.8 g/cm^3 (Weller et al., 2021). We note typical uncertainties of ± 0.1 GPa (~3 km) for geobarometric data (Spear, 1993).

Different provinces in the Southwest are characterized by distinct P-T paths summarized below and Figure S2. Metamorphism in the Yavapai and Mojave Provinces during the Yavapai orogeny is characterized by a looping P-T path with peak conditions of 0.6–0.7 GPa, 550–700 °C at 1.71–1.70 Ga followed by 0.2–0.3 GPa of decompression by 1.68 Ga (Williams and Karlstrom, 1996; Dumond et al., 2007; Mahan et al., 2013). Rocks in these provinces generally cooled isobarically in the mid-crust at 1.6–1.5 Ga until re-heating without significant additional burial during the ~1.45 Ga Picuris orogeny (Mahan et al., 2013). Peak pressures at ~1.70 Ga decrease southwards towards the Yavapai-Mazatzal transition zone where rocks were at or near the surface during the deposition of ~1.70 Ga quartzite and pelite successions (Jones et al., 2009). Supracrustal rocks of the Yavapai-Mazatzal transition zone and Mazatzal Province were deformed and buried to ~0.2–0.4 GPa during greenschist facies metamorphism in the Mazatzal orogeny with locally high temperatures near syn-tectonic plutons (Duebendorfer et al., 2015). During the Picuris orogeny, peak conditions reached amphibolite facies in the Yavapai-Mazatzal transition zone and Mazatzal Province with pressures of 0.3–0.4 GPa in New Mexico and up to ~0.6 GPa in south-central Colorado (Grambling, 1986; Daniel et al., 2023). This metamorphism has been interpreted in terms of a clockwise or looping P-T-t path (Grambling, 1986; Daniel et al., 2013).

At 1.72–1.69 Ga rocks exposed at the modern erosional surface were at depths of 15–25 km in eastern California, Grand Canyon, and northern Front Range (Fig. 6A; e.g. Dumond et al., 2007; Mahan et al., 2013), whereas the rocks in the Yavapai-Mazatzal transition zone were likely at or near the surface, as indicated by the deposition of ~1.70 Ga quartzite successions (Fig. 6A) (cf. Jones et al., 2009). The spatial pattern of greater burial depths to the north and decreasing burial depth to the south is nearly identical to the crustal thickness pattern at 1.72-1.69 Ga (Fig. 4A).

Geobarometric data constrained to 1.69–1.60 Ga suggest a N-S gradient in burial depth from ~10 km in the Mojave and Yavapai Provinces to ~5 km in the Yavapai-Mazatzal transition zone and Mazatzal Province at 1.69–1.60 Ga (Fig. 6B). This pattern is also qualitatively similar to the distribution of crustal thickness shown on Fig. 3B, with thicker crust in the Mojave and Yavapai Provinces relative to the Yavapai-Mazatzal transition zone and Mazatzal Province.

Burial depths at ~1.4 Ga were 3–12 km in eastern California, southern New Mexico, and central Colorado and increase in south-central Arizona and New Mexico (10–15 km) and the Wet Mountains of south-central Colorado (20–25 km) (Fig. 6B). This

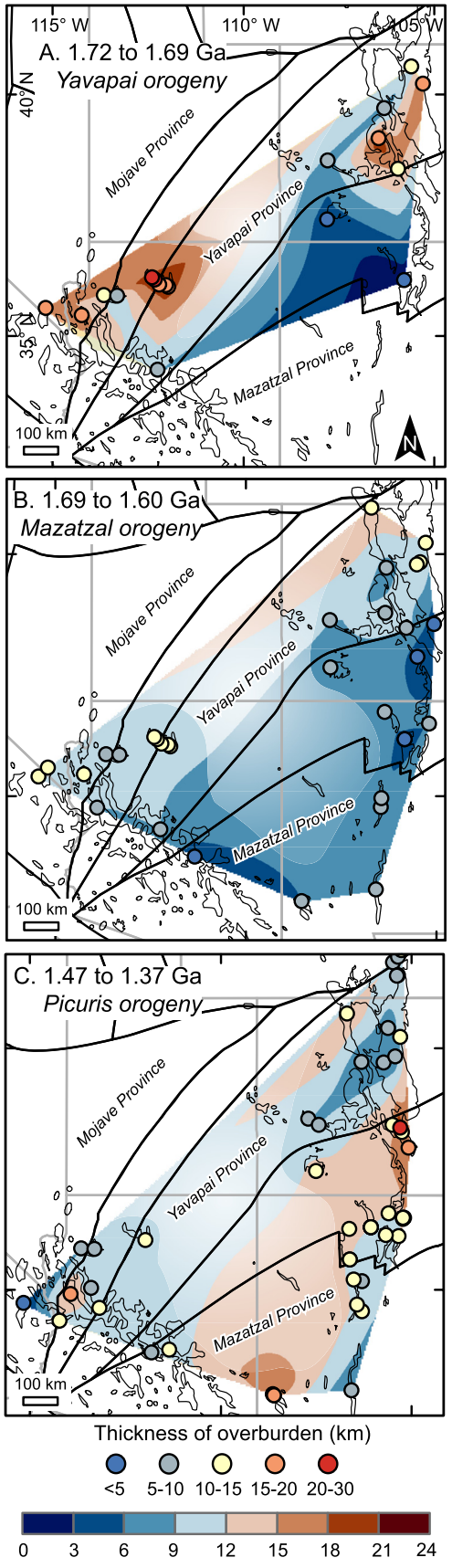

Fig. 6. Times slices of the metamorphic burial depth of rocks exposed at the modern erosional surface at 1.72-1.69 Ga (A), 1.69-1.60 Ga (B), and 1.47-1.37 Ga (C). Geobarometric data were converted to depth assuming a crustal density of 2.8 g/cm^3. Note: the opacity of the interpolated map is increased in areas where the dataset is more limited.

pattern of metamorphic pressures and burial depth is broadly consistent with crustal thickening in the Yavapai-Mazatzal transition zone and Mazatzal Province during the Picuris orogeny (Fig. 4C).

Collectively, patterns in geobarometric data and burial depth broadly match those of crustal thickness at similar times. We applied raster math calculations in ArcMap 10.8 for additional quantitative comparison of the geochemical crustal thickness proxies and burial depth and to evaluate where in the crustal column modification occurred (cf. Hillenbrand and Williams, 2021).

Fig. 7A shows the difference in burial depth of the modern erosional surface between 1.72–1.69 and 1.69–1.60 Ga. The map indicates the removal of 6–12 km of upper crust in the Mojave and Yavapai Provinces (cf. Dumond et al., 2007; Williams and Karlstrom, 1996). This correlates well with the results of geochemical proxies which suggest ~10 km of 1.70–1.68 Ga crustal thinning (Figs. 2A-B; 5B). Likewise, the moderate increase in burial depth (3–6 km) in southern Colorado and northern New Mexico accords with ~5–10 km of localized crustal thickening inferred from chemical mohometry (Figs. 2C; 5B).

Fig. 7B indicates that rocks of the Yavapai-Mazatzal transition zone and Mazatzal Province were overlain by 3–12 km of crust between ~1.60 Ga and ~1.45 Ga (Fig. 5C) and isobaric P-T paths indicate no change in burial depth in the Mojave and Yavapai Provinces (Williams and Karlstrom, 1996; Dumond et al., 2007; Mahan et al., 2013). These are significantly less than the ~10–20 km of crustal thickening in this interval and require crustal thickening below the present erosion surface (i.e., broadly in the lower crust) at the time of metamorphism. Fig. 7C shows the results of raster math calculations that estimate the amount and spatial distribution of change in the thickness of the crustal column below the present erosion surface between 1.69–1.60 Ga and ~1.45 Ga. Coupled chemical mohometric and barometric constraints suggest 6–12 km of crustal thickening below the present erosional surface across much of the Southwest (Fig. 7C).

6. Discussion and implications

6.1. Comparison and integration of chemical mohometry and geobarometry

The spatial patterns of burial depth and crustal thickness show broad consistency (Figs. 4, 6). We also observe concordant magnitudes of change in burial depth and crustal thickness (Figs. 5, 7). The correlations between these independent methods significantly strengthens our confidence in the application of chemical mohometry. As described below, these datasets can be combined to gain greater insights into orogenic and crustal evolution.

The 1.72–1.69 Ga Yavapai orogeny has been interpreted to be associated with the accretion of the Yavapai and Mojave Provinces to the composite margin of Laurentia. The degree of 1.72–1.69 Ga crustal thickening shown in Fig. 5A generally matches the 1.72–1.69 Ga increase in burial depth as seen on Fig. 6A. This suggests burial of rocks exposed at the modern erosional surface by processes including crustal shortening, thrusting, and folding in the upper ~25 km of the crust can largely account for crustal thickening during this event. This inference accords with structural and petrologic studies that record mid- and upper crustal shortening, thrusting, and folding during the Yavapai orogeny (Hawkins et al., 1996; Dumond et al., 2007; Mahan et al., 2013). Similarly, ~10 km of crustal thinning between 1.70 and 1.68 Ga in the Yavapai and Mojave Provinces indicated by chemical mohometry (Fig. 5B) agrees well with the spatial extent and amount of exhumation suggested by 0.2–0.3 GPa of decompression in the same region (Fig. 7B) (Williams and Karlstrom, 1996; Dumond et al., 2007; Mahan et al., 2013). Thus, thickness changes during and immediately after the Yavapai orogeny, involving contractional and then

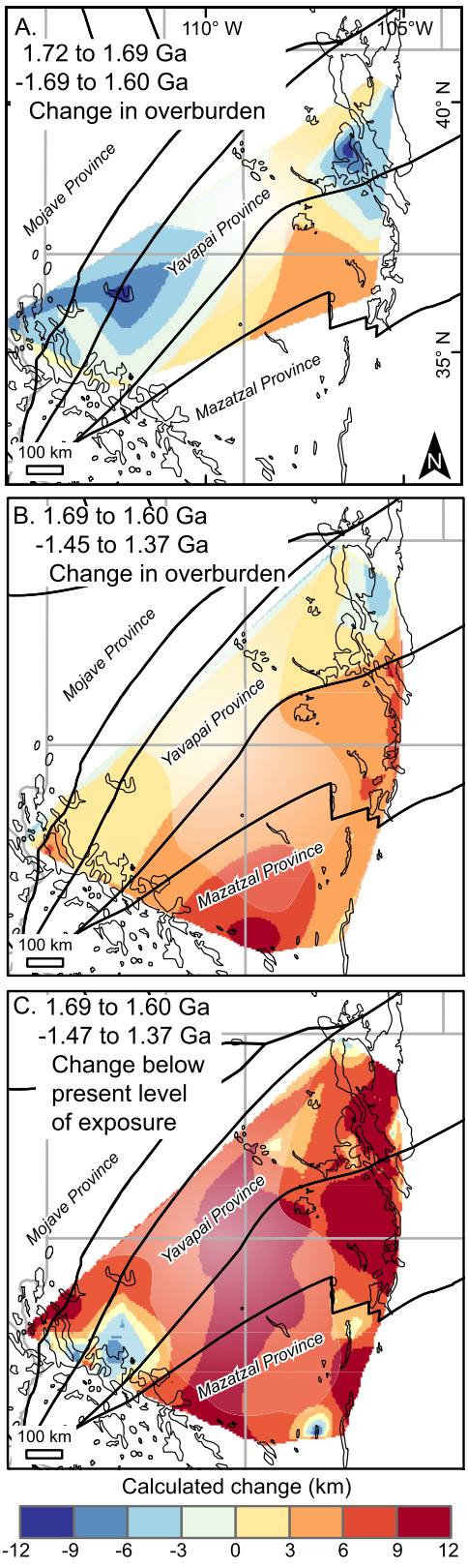

Fig. 7. Geobarometric constraints on burial depth. (A) Change in burial depth between 1.72-1.69 Ga and 1.69-1.60 Ga. Note ~10 km of thinning due to extension and/or erosion in Grand Canyon and central Colorado. (B) Change in burial depth of the between 1.69-1.60 Ga and 1.47-1.37 Ga. (C) Change in thickness of the crust below the present erosional surface between the 1.69-1.60 Ga and 1.47-1.37 Ga time slices. Note that the constraints are primarily from basement exposures (shown as outlines) and lesser confidence is placed on in the intervening areas which have fewer constraints. Note: the opacity of the interpolated map is increased in areas where the dataset is more limited.

erosion and extensional tectonism, occurred largely at or above the modern erosional surface (i.e., in the upper ~25 km of the crust).

In contrast, data from the 1.47–1.37 Ga Picuris orogeny indicate that increasing burial depth of the modern erosional surface cannot fully account for crustal thickening indicated by chemical mohometry (Fig. 7). The data require ~6–12 km of crustal thickening below the current exposure level of metamorphic rocks, particularly in the Yavapai and Mojave Provinces (Fig. 7C). This may be explained by petrogenetic models for the generation of the widespread ~1.4 Ga granitoids (Frost and Frost, 1997, 2023; Keller et al., 2005). Isotopic mass balance models for the genesis of ~1.4 Ga ferroan granites in the Southwest involve the addition of 5–10 km of basaltic (tholeiitic) material via underplating in the lower crust (Frost et al., 2001). Lithospheric-scale seismic studies have imaged a high-velocity (up to 7.0–7.5 km/s) ~10 km thick layer at the base of the crust throughout the southwestern United States which has been interpreted as underplated mafic material (Keller et al., 2005). Studies of deep crustal xenoliths from the Colorado Front Range (Farmer et al., 2005) and Four Corners (Crowley et al., 2006) have yielded isotopically juvenile, ~1.4 Ga mafic granulites that have been interpreted as directly documenting a mafic underplate. Likewise the Sm-Nd isotopic systematics of mantle xenoliths from the Colorado Plateau are consistent with significant melt production at ~1.4 Ga (Marshall et al., 2017). Collectively, we interpret this to suggest magmatic underplating played an important role in crustal thickening during the Picuris orogeny.

6.2. Evolving Proterozoic orogenic styles in the Southwest

Samples dated to 1.84–1.72 Ga largely yielded crustal thickness estimates between 25 and 40 km (Figs. 2–3). These values are similar to modern day island and continental arcs (cf. Luffi and Ducea, 2022), consistent with previous interpretations from geologic constraints and largely juvenile isotopic data (Karlstrom and Bowring, 1988; Bowring and Karlstrom, 1990; Jessup et al., 2005; Jones et al., 2011; Baird et al., 2022). Locally, the data suggest thinning, particularly in the Yavapai Province between 1.78 and 1.75 Ga, which is consistent with models that involve the formation of new juvenile arcs and back-arc extension (Jessup et al., 2005; Jones et al., 2011; Baird et al., 2022). Slightly thicker crust, ~40 km, at ~1.76 Ga in the vicinity of the Cheyenne belt is consistent with the accretion of the Green Mountain arc to the Archean Wyoming Province during the Medicine Bow orogeny (Chamberlain, 1998; Jones et al., 2011). Crustal thickening to 50-55 km in the Mojave Province at 1.76–1.74 Ga suggests localized tectonism and, possibly, collision of the Yavapai and Mojave Provinces (Duebendorfer et al., 2001; Holland et al., 2018). We interpret tectonism in this period to involve the formation of arc terranes, back-arc extension, and local collision of arc and back-arc terranes, perhaps comparable in some ways to present Indonesia (Jessup et al., 2005).

Crustal thickening to 50-60 km at 1.72–1.69 Ga occurred in the Yavapai and Mojave Provinces, a relatively narrow belt, for a duration of ~20–30 m.y. (Figs. 2, 4). Geobarometric data, when compared with igneous geochemical crustal thickness proxies, indicate that both crustal thickening and thinning associated with the Yavapai orogeny can be explained by burial, shortening, and subsequent exhumation (Figs. 5, 7). These inferences are consistent with geologic and structural evidence for shortening, folding, and thrusting in the upper ~25 km of the crust (Williams and Karlstrom, 1996; Karlstrom and Williams, 1998; Dumond et al., 2007; Mahan et al., 2013) as indicated on Fig. 8A.

The new crustal thickness data also provide a solution to a long-lived debate regarding the depositional setting of 1-2 km thick successions of quartzite and pelites, such as the Ortega and Uncompaghre Formations, in the southern Yavapai Province (e.g. Jones et al., 2009) (Fig. 1). Recent geochronologic constraints (Karlstrom et al., 2017; Hillenbrand et al., 2023 and references therein) show that these successions were deposited at ~1.70 ± 0.1 Ga. Fig. 3A shows relatively thin crust (~35 km) almost exactly corresponding to the region of quartzite and pelite deposition in the southern Yavapai Province adjacent to significantly thicker (50-60 km) crust to the north. We suggest that deposition in these basins was synchronous with, or immediately followed, crustal thickening and accretion of the Yavapai Province to the Laurentian craton during the Yavapai orogeny, as shown schematically on Fig. 8A. The relatively short-lived duration of the ~1.75 and ~1.70 Ga crustal thickening events and contemporaneous deposition of quartzite and pelite successions are consistent with numerical models for hotter Proterozoic orogenesis that predict greater slab rollback and/or shallower slab breakoff following collision (Sizova et al., 2014; Chowdhury et al., 2020, 2021; Baird et al., 2022). The relatively sharp gradients in crustal thickness and burial depth at ~1.70 Ga imply that the crust was rheologically strong enough to maintain significant topographic gradients (Karlstrom and Williams, 1998; Keller et al., 2005).

The period associated with the Mazatzal orogeny (1.68–1.60 Ga) is characterized by relatively thin crust (25–40 km) in the Mazatzal Province (Fig. 4B), local crustal thickening on the order of 5-10 km in the Yavapai-Mazatzal transition zone, and ~10 km of crustal thinning the Yavapai and Mojave Provinces (Fig. 5B). Local crustal thickening on the order of 5-10 km conforms with the generally greenschist facies, low-P, and variable-T metamorphism associated with Mazatzal orogeny (Duebendorfer et al., 2015; Karlstrom et al., 2016; Holland et al., 2020). Diachronous low-P, variable-T metamorphism, moderate amounts of generally localized crustal shortening and crustal thickening, the widespread occurrence of granites and silicic volcanics, and deposition in continental to shallow marine basins (Duebendorfer et al., 2015; Holland et al., 2020) suggest an extensional accretionary orogen as described by Collins (2002). As shown on Fig. 8B, we envision a scenario involving continental arc magmatism and variable angle subduction in an accretionary orogenic setting (cf. Holland et al., 2020) to explain the available observations. The lull of magmatism and tectonism between 1.6 and 1.5 Ga has been interpreted to reflect a change from a dominance of convergence to strike slip along the southern margin of Laurentia which was located south of New Mexico (Karlstrom et al., 2004; Holland et al., 2020; Daniel et al., 2023).

The Mesoproterozoic Picuris orogeny in the Southwest contrasts with the earlier tectonism as it is associated with a much larger region of 50–60 km thick crust and a longer duration (50–80 m.y.) of thick crust (Figs. 2; 4C). The Picuris orogeny also differs from the earlier Yavapai orogeny and Mazatzal orogeny in terms of the major processes associated with crustal thickening. In addition to mid- to upper-crustal shortening, 5–10 km of crustal thickening occurred in the lower crust, likely via magmatic underplating, a scenario visualized on Fig. 8C. The greatest crustal thickening, burial, and most intense deformation during the Picuris orogeny took place in the Yavapai-Mazatzal transition zone and Mazatzal Province which at 1.7–1.6 Ga were underlain by relatively thin (~30 km) crust and had sedimentary basins. In contrast, the Yavapai and Mojave Provinces experienced little ~1.4 Ga burial; the relatively more localized deformation and metamorphism in these regions was largely associated with (re)activation of shear zones and the contact aureoles of ~1.4 Ga plutons (McCoy et al., 2005; Shaw et al., 2005; Mahan et al., 2013; Hillenbrand et al., 2023). Fig. 8C shows a schematic model integrating mohometric and petrologic data with geologic constraints, involving a broad region of 50–60 km thick crust, widespread lower crustal magmatic underplating, and, at higher crustal levels, a transition from more localized to regional shortening from north to south.

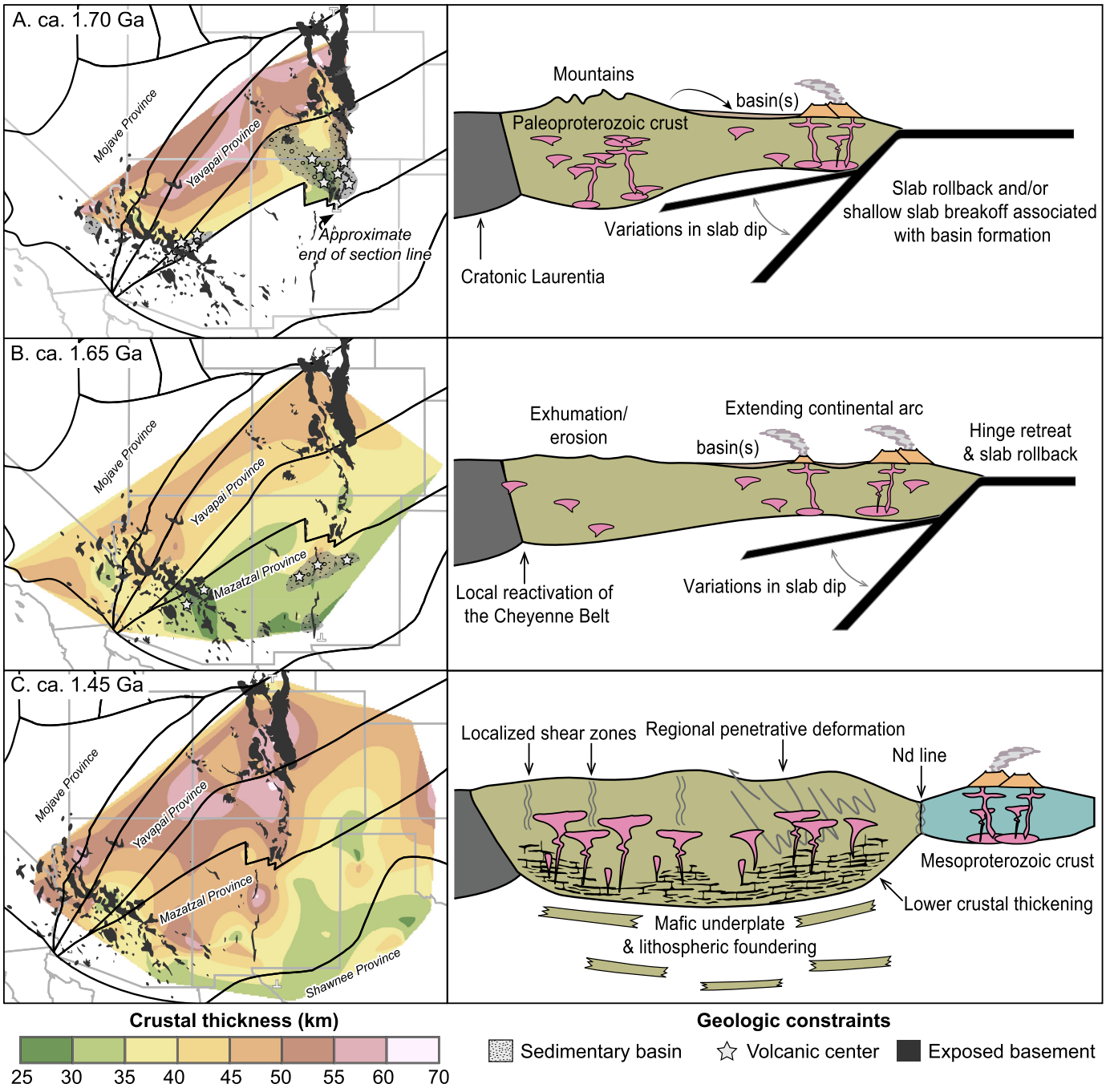

Fig. 8. Simplified maps of crustal thickness and geologic constraints and associated interpreted tectonic cross sections at ~1.70 Ga (A), ~1.65 Ga (B), and ~1.45 Ga (C). The cross sections generally follow the N-S line of Shaw et al. (2005) and are approximated on the maps by tick marks.

Our results provide context for, and may help to explain, ongoing controversy regarding the extent of, and N-S differences, in the style of deformation and extent of crustal shortening during the ca. 1.47–1.37 Ga Picuris orogeny (Shaw et al., 2005; Daniel et al., 2013, 2023). Our data indicate that more intense shortening and tectonometamorphism associated with the Picuris orogeny occurred in areas of previously relatively thin (~30 km) crust at 1.7–1.6 Ga (the Yavapai-Mazatzal transition zone and Mazatzal Province). This thinner, and likely rheologically weaker, crust may have been more prone to accommodating shortening relative to the thicker (~40 km), colder, older, and likely rheologically stronger Yavapai and Mojave Provinces which may have acted as a buttress.

Overall, the lack of sharp boundaries in crustal thickness at ca. 1.4 Ga (Figs. 4c, 8c) compared to ca. 1.7 Ga (Figs. 4a, 8a) is compatible with a relatively hotter and weaker crust. Sustaining a thickened, rheologically weak crust likely requires continued compressional stress (Hillenbrand et al., 2021; Weller et al., 2021). Convergence at 1.47–1.37 Ga may have been provided by protracted shallow subduction under Laurentia and/or accretion of the Shawnee Province (Bickford et al., 2015; Daniel et al., 2023). The broad region of 50-60 km thick crust, smooth gradients in burial depth, and thermochronologic evidence for slow cooling are consistent with models suggested by Keller et al. (2005) and Shaw et al. (2005) involving a ca. 1.4 Ga orogenic plateau.

6.3. Mesoproterozoic basaltic underplating and high crustal geotherms in the Southwest

The intrusion of basaltic magmas at ca. 1.4 Ga in the lower crust was likely associated with melting of the lower crust and genesis of ferroan granitic magmas (Frost and Frost, 1997; Frost et al., 2001). The emplacement of granitic magmas into the mid-crust would have advected heat into the mid-crust, raising apparent geothermal gradients (Williams et al., 1999; Shaw et al., 2005). High crustal temperatures, supported by heat associated with basaltic underplating and emplacement of granitic magmas, and partial melting at ca. 1.4 Ga would be expected to weaken the crust (Karlstrom and Williams, 1998; Hillenbrand et al., 2021; Gorczyk and Vogt, 2015), consistent with the lack of sharp gradients in crustal thickness (Fig. 4C) and metamorphic pressures (Fig. 6C; cf. Grambling, 1986).

Mesoproterozoic ferroan granites were emplaced in a >4,000-km-long belt across Laurentia and Baltica along the active leading margin of the supercontinent Nuna (Columbia) (Anderson and Morrison, 2005; Daniel et al., 2023; Frost and Frost, 2023). The abundance of ferroan granites suggests extensive basaltic underplating (Frost et al., 2001). The drivers of this process likely included the removal (foundering) of eclogitic lithospheric material due to lithospheric shortening (Gorczyk and Vogt, 2015), heating due to continental insulation under Nuna (Columbia), and/or a back-arc tectonic setting (Condie, 2013; Bickford et al., 2015; Roberts et al., 2022; Frost and Frost, 2023). Regardless of mechanism(s), basaltic underplating and associated advective heating of the mid-crust during ferroan pluton emplacement are consistent with, and may explain some of, the elevated geothermal gradients and inferred changes in surface topography in the middle Proterozoic (Frost et al., 2001; Spencer et al., 2021; Roberts et al., 2022).

6.4. Challenges and strategies for deep time chemical mohometry

Deep time applications of chemical mohometry involve assumptions of broadly uniformitarian petrogenetic processes. It has been suggested that the average composition of the continental crust deep in Earth's past differed from the present, either due to changes in the tectonic setting associated with crust formation or secular changes such as variability in mantle temperature (Keller and Schoene, 2018 and references therein). Changes in the mantle temperature, for example, are interpreted to be associated with smooth trends of decreasing compatible and increasing compatible elements of the past 4 Ga, with smaller changes over the last 2 Ga (Keller and Schoene, 2012, 2018 and references therein). Hence, it is possible that these changes affect, to some extent, the accuracy of individual mohometers in deep time. This effect may be more impactful for individual mohometers (Keller and Harrison, 2020), as no single mohometer is expected to reveal optimal crustal thickness estimates in all settings (Luffi and Ducea, 2022), and individual calibrations having varying compatibility during mantle melting (Luffi and Ducea, 2022).

Luffi and Ducea (2022) calibrated 41 mohometers that vary in their compatibility and sensitivity to crustal differentiation. Hence, multiple crustal thickness proxies can be applied to evaluate and potentially minimize possible biases in the dataset. Consistent values from multiple proxies may be indicative of results that are more robust than any single whole-rock or mineral proxy. In cases where partitioning coefficients are similar, it is possible that these proxies, or multiple proxies, may still yield insights regarding *relative* crustal thickness changes. Evaluation and validation of absolute changes may be carried out in cases where independent petrologic and geologic constraints on crustal thickness and crustal thickness change are available. Independent constraints on depth may come from thermobarometric data (e.g. this study, Hillenbrand and Williams, 2021) or thermochronology in less deeply exhumed terranes (e.g. Jepson et al., 2022). The correspondence of multiproxy chemical mohometry with geobarometry and the sedimentary rock record in this study indicates that the multiproxy approach is reasonably accurate and robust in this case. We suggest that comparison of chemical mohometric and geobarometric data is an important process step in assessing the accuracy of the deep time chemical mohometry and applicability. The correlation we observe between chemical mohometry and geobarometry may support the results of Keller and Schoene (2018, 2012) that element partitioning was not significantly different at 1.8–1.4 Ga.

7. Conclusions

In this contribution we quantified the Proterozoic crustal thickness record of the southwestern U.S.A. using whole rock igneous geochemical proxies. The calculations indicate at least four phases of crustal thickening characterized by different orogenic styles. The relatively short duration of crustal thickening and contemporaneous basin formation at ~1.70 Ga is consistent with arrested orogenesis associated with shallow slab breakoff and rollback. Subsequent tectonism at 1.69–1.60 Ga supports an extensional accretionary orogen model. The 1.47–1.37 Ga Picuris orogeny was associated with widespread crustal thickening to 50-60 km across much of the Southwest and involved crustal shortening and magmatic underplating. Advective heat from the mid-crustal emplacement of ferroan granites may have contributed to the elevated geothermal gradients and rheologically weak crust in the middle Proterozoic.

We show that high spatial and temporal resolution crustal thickness records are a powerful tool to broadly evaluate crustal evolution in ancient orogens, particularly when integrated with geobarometric constraints. An approach integrating igneous geochemical crustal thickness constraints with geobarometric data can be widely applied to ancient and more recent orogens to understand crustal evolution and lower crustal processes. Although our results are from a single, albeit significant, middle Proterozoic orogenic belt, they suggest this period was neither orogenically quiescent or tectonically stagnant; rather, they indicate a dynamic 500 m.y. period of crustal evolution with complex and contrasting mountain building styles.

CRediT authorship contribution statement

Ian W. Hillenbrand: Writing – review & editing, Writing – original draft, Visualization, Validation, Methodology, Investigation, Formal analysis, Data curation, Conceptualization. **Karl E. Karlstrom:** Writing – review & editing, Investigation, Conceptualization. **Michael L. Williams:** Writing – review & editing, Visualization, Investigation, Conceptualization. **Amy Gilmer:** Writing – review & editing, Visualization, Resources, Investigation, Funding acquisition. **Wayne Premo:** Investigation. **Peter Davis:** Writing – review & editing, Investigation.

Declaration of competing interest

The authors declare that they have no known competing financial interests or personal relationships that could have appeared to influence the work reported in this paper.

Data availability

Compiled geochemical and geobarometry data and the results of mohometric calculations are provided in the Supplemental Material. Recently published geochemical and geochronologic con-

straints used in this study are provided via a U.S. Geological Survey data release (Premo et al., 2023).

Acknowledgements

IWH and AKG were supported by the U.S. Geological Survey National Cooperative Geologic Mapping Program. Any use of trade, firm, or product names is for descriptive purposes only and does not imply endorsement by the U.S. Government. KEK acknowledges partial support from NSF EAR-9508096, 9614787, 0003500, and 1145247. We appreciate comments by Gilby Jepson, Greg Walsh, and an anonymous reviewer, the USGS geologic names review of Kelly Thomson, and the editorial handling of Alex Webb. We thank J.V. Jones and three anonymous reviewers for comments on an earlier version of this manuscript.

Appendix A. Supplementary material

Supplementary material related to this article can be found online at https://doi.org/10.1016/j.epsl.2023.118417.

References

Anderson, J.L., Morrison, J., 2005. Ilmenite, magnetite, and peraluminous Mesoproterozoic anorogenic granites of Laurentia and Baltica. Lithos 80, 45–60. https://doi.org/10.1016/j.lithos.2004.05.008.

Baird, G.B., Grover, T.W., Mahan, K.H., Frothingham, M.G., Raschke, M.B., Möller, A., Chumley, A.S., Hooker, J.C., Kelly, N.M., Allaz, J.M., 2022. Paleoproterozoic tectonics of the northern Colorado Rocky Mountains Front Range, USA. In: Mahan, K.H., Carpenter, L. (Eds.), Field Excursions in the Front Range and Wet Mountains of Colorado for GSA Connects 2022. Geological Society of America, pp. 39–66.

Barnes, M.A., Rohs, C.R., Anthony, E.Y., Van Schmus, W.R., Denison, R.E., 1999. Isotopic and elemental chemistry of subsurface Precambrian igneous rocks, west Texas and eastern New Mexico. Rocky Mt. Geol. 34, 245–262. https://doi.org/10.2113/34.2.245.

Bennett, V.C., DePaolo, D.J., 1987. Proterozoic crustal history of the western United States as determined by neodymium isotopic mapping. Geol. Soc. Am. Bull. 99, 674–685. https://doi.org/10.1130/0016-7606(1987)99<674:PCHOTW>2.0.CO;2.

Bickford, M.E., Van Schmus, W.R., Karlstrom, K.E., Mueller, P.A., Kamenov, G.D., 2015. Mesoproterozoic-trans-Laurentian magmatism: a synthesis of continent-wide age distributions, new SIMS U-Pb ages, zircon saturation temperatures, and Hf and Nd isotopic compositions. Precambrian Res. 265, 286–312. https://doi.org/10.1016/j.precamres.2014.11.024.

Bowring, S.A., Karlstrom, K.E., 1990. Growth, stabilization, and reactivation of Proterozoic lithosphere in the southwestern United States. Geology 18, 1203–1206. https://doi.org/10.1130/0091-7613(1990)018<1203:GSAROP>2.3.CO;2.

Carmichael, D.M., 1978. Metamorphic bathozones and bathograds; a measure of the depth of post-metamorphic uplift and erosion on the regional scale. Am. J. Sci. 278, 769–797. https://doi.org/10.2475/ajs.278.6.769.

Chamberlain, K.R., 1998. Medicine Bow orogeny: timing of deformation and model of crustal structure produced during continent-arc collision, ca. 1.78 Ga, southeastern Wyoming. Rocky Mt. Geol. 33, 259–277. https://doi.org/10.2113/33.2.259.

Chowdhury, P., Chakraborty, S., Gerya, T.V., Cawood, P.A., Capitanio, F.A., 2020. Peel-back controlled lithospheric convergence explains the secular transitions in Archean metamorphism and magmatism. Earth Planet. Sci. Lett. 538, 116224. https://doi.org/10.1016/j.epsl.2020.116224.

Chowdhury, P., Chakraborty, S., Gerya, T.V., 2021. Time will tell: secular change in metamorphic timescales and the tectonic implications. Gondwana Res. 93, 291–310. https://doi.org/10.1016/j.gr.2021.02.003.

Collins, W.J., 2002. Nature of extensional accretionary orogens. Tectonics 21, 6–1–6–12. https://doi.org/10.1029/2000TC001272.

Condie, K.C., 1982. Plate-tectonics model for Proterozoic continental accretion in the southwestern United States. Geology 10, 37–42. https://doi.org/10.1130/0091-7613(1982)10<37:PMFPCA>2.0.CO;2.

Condie, K.C., 2013. Preservation and recycling of crust during accretionary and collisional phases of Proterozoic orogens: a bumpy road from nuna to rodinia. Geosciences 3, 240–261. https://doi.org/10.3390/geosciences3020240.

Corrigan, D., Pehrsson, S., Wodicka, N., de Kemp, E., 2009. The Palaeoproterozoic Trans-Hudson Orogen: a prototype of modern accretionary processes. In: Murphy, J.B., Keppie, J.D., Hynes, A.J. (Eds.), Ancient Orogens and Modern Analogues. Geological Society Special Publication, pp. 457–479.

Crowley, J.L., Schmitz, M.D., Bowring, S.A., Williams, M.L., Karlstrom, K.E., 2006. U-Pb and Hf isotopic analysis of zircon in lower crustal xenoliths from the Navajo volcanic field: 1.4 Ga mafic magmatism and metamorphism beneath the Colorado Plateau. Contrib. Mineral. Petrol. 151, 313–330. https://doi.org/10.1007/s00410-006-0061-z.

Daniel, C.G., Pfeifer, L.S., Jones, J.V., McFarlane, C.M., 2013. Detrital zircon evidence for non-Laurentian provenance, Mesoproterozoic (ca. 1490-1450 Ma) deposition and orogenesis in a reconstructed orogenic belt, northern New Mexico, USA: defining the Picuris orogeny. Geol. Soc. Am. Bull. 125, 1423–1441. https://doi.org/10.1130/B30804.1.

Daniel, C.G., Aronoff, R., Indares, A., Jones III, J.V., 2023. Laurentia in transition during the Mesoproterozoic: observations and speculation on the ca. 1500–1340 Ma tectonic evolution of the southern Laurentian margin. In: Whitmeyer, S.J., Williams, M.L., Kellett, D.A., Tikoff, B. (Eds.), Laurentia: Turning Points in the Evolution of a Continent. Geological Society of America.

Doe, M.F., Jones, J.V., Karlstrom, K.E., Thrane, K., Frei, D., Gehrels, G., Pecha, M., 2012. Basin formation near the end of the 1.60-1.45 Ga tectonic gap in southern Laurentia: Mesoproterozoic Hess Canyon Group of Arizona and implications for ca. 1.5 Ga supercontinent configurations. Lithosphere 4, 77–88. https://doi.org/10.1130/L160.1.

du Bray, E.A., Holm-Denoma, C.S., San Juan, C.A., Lund, K., Premo, W.R., DeWitt, E., 2015. Geochemical, modal, and geochronologic data for 1.4 Ga A-type granitoid intrusions of the conterminous United States, Data Series. Reston, VA. https://doi.org/10.3133/ds942.

Duebendorfer, E.M., Chamberlain, K.R., Jones, C.S., 2001. Paleoproterozoic tectonic history of the Cerbat Mountains northwestern Arizona: implications for crustal assembly in the southwestern United States. GSA Bull. 113, 575–590. https://doi.org/10.1130/0016-7606(2001)113<0575:PTHOTC>2.0.CO;2.

Duebendorfer, E.M., Williams, M.L., Chamberlain, K.R., 2015. Case for a temporally and spatially expanded Mazatzal orogeny. Lithosphere 7, 603–610. https://doi.org/10.1130/L412.1.

Dumond, G., Mahan, K.H., Williams, M.L., Karlstrom, K.E., 2007. Crustal segmentation, composite looping pressure-temperature paths, and magma-enhanced metamorphic field gradients: Upper Granite Gorge, Grand Canyon, USA. Bull. Geol. Soc. Am. 119, 202–220. https://doi.org/10.1130/B25903.1.

Farmer, G.L., Samuel, A., Williams, M.L., Stevens, L., 2005. Contrasting lower crustal evolution across an Archean-Proterozoic suture: physical, chemical and geochronologic studies of lower crustal xenoliths in Southern Wyoming and Northern Colorado. In: Karlstrom, K.E., Keller, G.R. (Eds.), The Rocky Mountain Region: An Evolving Lithosphere. American Geophysical Union.

Frost, C.D., Frost, B.R., 1997. Reduced rapakivi-type granites: the tholeiite connection. Geology 25, 647–650. https://doi.org/10.1130/0091-7613(1997)025<0647:RRTGTT>2.3.CO;2.

Frost, C.D., Frost, B.R., 2023. Proterozoic ferroan granites of the Laurentian margin. In: Whitmeyer, S.J., Williams, M.L., Kellett, D.A., Tikoff, B. (Eds.), Laurentia: Turning Points in the Evolution of a Continent: Geological Society of America Memoir 220. Geological Society of America, Boulder, Colorado, pp. 1–24.

Frost, C.D., Bell, J.M., Frost, B.R., Chamberlain, K.R., 2001. Crustal growth by magmatic underplating: isotopic evidence from the northern Sherman batholith. Geology 29, 515–518. https://doi.org/10.1130/0091-7613(2001)029<0515:CGBMUI>2.0.CO;2.

Gorczyk, W., Vogt, K., 2015. Tectonics and melting in intra-continental settings. Gondwana Res. 27, 196–208. https://doi.org/10.1016/j.gr.2013.09.021.

Grambling, J.A., 1986. Crustal thickening during Proterozoic metamorphism and deformation in New Mexico. Geology 14, 149–152. https://doi.org/10.1130/0091-7613(1986)14<149:CTDPMA>2.0.CO;2.

Hawkins, D.P., Bowring, S.A., Ilg, B.R., Karlstrom, K.E., Williams, M.L., 1996. U-Pb geochronologic constraints on the Paleoproterozoic crustal evolution of the Upper Granite Gorge, Grand Canyon, Arizona. Geol. Soc. Am. Bull. 108, 1167–1181. https://doi.org/10.1130/0016-7606(1996)108<1167:UPGCOT>2.3.CO;2.

Hillenbrand, I.W., Williams, M.L., 2021. Paleozoic evolution of crustal thickness and elevation in the northern Appalachian orogen, USA. Geology 49, 946–951. https://doi.org/10.1130/G48705.1.

Hillenbrand, I.W., Williams, M.L., 2022. Geochemical evidence for diachronous uplift and synchronous collapse of the high elevation Variscan hinterland. Geophys. Res. Lett. 49, e2022GL100435. https://doi.org/10.1029/2022GL100435.

Hillenbrand, I.W., Williams, M.L., Li, C., Gao, H., 2021. Rise and fall of the Acadian altiplano: evidence for a Paleozoic orogenic plateau in New England. Earth Planet. Sci. Lett. 560. https://doi.org/10.1016/j.epsl.2021.116797.

Hillenbrand, I.W., Williams, M.L., Karlstrom, K.E., Gilmer, A.K., Lowers, H.A., Jercinovic, M.J., Suarez, K.A., Souders, A.K., 2023. Monazite and xenotime petrochronologic constraints on four Proterozoic tectonic episodes and ca. 1705 Ma age of the Uncompahgre Formation, southwestern Colorado. Geosphere 49. https://doi.org/10.1130/GES02631.1.

Holland, M.E., Karlstrom, K.E., Gehrels, G., Shufeldt, O.P., Begg, G., Griffin, W., Belousova, E., 2018. The Paleoproterozoic Vishnu basin in southwestern Laurentia: Implications for supercontinent reconstructions, crustal growth, and the origin of the Mojave crustal province. Precambrian Res. 308, 1–17. https://doi.org/10.1016/j.precamres.2018.02.001.

Holland, M.E., Grambling, T.A., Karlstrom, K.E., Jones, J.V., Nagotko, K.N., Daniel, C.G., 2020. Geochronologic and Hf-isotope framework of Proterozoic rocks from central New Mexico, USA: formation of the Mazatzal crustal province in an extended continental margin arc. Precambrian Res. 347, 105820. https://doi.org/10.1016/j.precamres.2020.105820.

Jepson, G., et al., 2022. Where did the Arizona-plano go? Protracted thinning via upper- to lower-crustal processes. J. Geophys. Res., Solid Earth 127, e2021JB023850. https://doi.org/10.1029/2021JB023850.

Jessup, M.J., Karlstrom, K.E., Connelly, J., Williams, M., Livaccari, R., Tyson, A., Rogers, S.A., 2005. Complex Proterozoic crustal assembly of southwestern North America in an arcuate subduction system: the Black Canyon of the Gunnison, southwestern Colorado. In: Karlstrom, K.E., Keller, G.R. (Eds.), Geophysical Monograph Series. American Geophysical Union, Washington, D. C., pp. 21–38.

Jones, D.S., Barnes, C.G., Premo, W.R., Snoke, A.W., 2011. The geochemistry and petrogenesis of the Paleoproterozoic Green Mountain arc: a composite(?), bimodal, oceanic, fringing arc. Precambrian Res. 185, 231–249. https://doi.org/10.1016/j.precamres.2011.01.011.

Jones III, J.V., Daniel, C.G., 2023. Circa 1.50–1.45 Ga metasedimentary rocks in southwestern Laurentia provide distinctive records of Mesoproterozoic regional orogenesis and craton interactions. In: Whitmeyer, S.J., Williams, M.L., Kellett, D.A., Tikoff, B. (Eds.), Laurentia: Turning Points in the Evolution of a Continent. Geological Society of America.

Jones, J.V., Connelly, J.N., Karlstrom, K.E., Williams, M.L., Doe, M.F., 2009. Age, provenance, and tectonic setting of Paleoproterozoic quartzite successions in the southwestern United States. Geol. Soc. Am. Bull. 121, 247–264. https://doi.org/10.1130/B26351.1.

Karlstrom, K., Amato, J., Williams, M., Heizler, M., Shaw, C., Read, A., Bauer, P., Mack, G., Giles, K., 2004. Proterozoic Tectonic Evolution of the New Mexico Region: A Synthesis. The Geology of New Mexico: A Geologic History: New. Mexico Geological Society Special Publication, vol. 11, pp. 1–34.

Karlstrom, K.E., Bowring, S.A., 1988. Early Proterozoic assembly of tectonostratigraphic terranes in southwestern North America. J. Geol. 96, 561–576. https://doi.org/10.1086/629252.

Karlstrom, K.E., Williams, M.L., 1998. Heterogeneity of the middle crust: implications for strength of continental lithosphere. Geology 26, 815. https://doi.org/10.1130/0091-7613(1998)026<0815:HOTMCI>2.3.CO;2.

Karlstrom, K.E., Williams, M.L., Heizler, M.T., Amato, J.M., 2016. U-Pb Monazite and 40Ar/39Ar data supporting polyphase tectonism in the Manzano Mountains: a record of both the Mazatzal (1.66-1.60 Ga) and Picuris (1.45 Ga) Orogenies. In: Frey, B.A., Karlstrom, K.E., Lucas, S.G., Williams, S., Ziegler, K., McLemore, V., Ulmer-Scholle, D.S. (Eds.), New Mexico Geological Society Fall Field Conference Guidebook – 67 The Geology of the Belen Area, pp. 177–184.

Karlstrom, K.E., Gonzales, D.A., Simmerer, M.J., Heizler, M., Ulmer-Scholle, D.S., 2017. 40Ar/39Ar age constraints on the deposition and metamorphism of the Uncompahgre Group, southwestern Colorado. In: New Mexico Geological Society Guidebook, 68th Field Conference, Geology of the Ouray-Silverton Area, pp. 85–92.

Keller, B., Schoene, B., 2018. Plate tectonics and continental basaltic geochemistry throughout Earth history. Earth Planet. Sci. Lett. 481, 290–304. https://doi.org/10.1016/j.epsl.2017.10.031.

Keller, C.B., Harrison, T.M., 2020. Constraining crustal silica on ancient Earth. Proc. Natl. Acad. Sci. USA 117, 21101–21107. https://doi.org/10.1073/pnas.2009431117.

Keller, C.B., Schoene, B., 2012. Statistical geochemistry reveals disruption in secular lithospheric evolution about 2.5 Gyr ago. Nature 485, 490–493. https://doi.org/10.1038/nature11024.

Keller, G.R., Karlstrom, K.E., Williams, M.L., Miller, K.C., Andronicos, C., Levander, A.R., Snelson, C.M., Prodehl, C., 2005. The dynamic nature of the continental crust-mantle boundary: crustal evolution in the southern rocky mountain region as an example. In: The Rocky Mountain Region: An Evolving Lithosphere. In: Geophysical Monograph Series, pp. 403–420.

Kirkland, C., Spaggiari, C., Wingate, M., Smithies, R., Belousova, E., Murphy, R., Pawley, M., 2011. Inferences on crust–mantle interaction from Lu–Hf isotopes: a case study from the Albany–Fraser Orogen. Geol. Surv. West. Aust. Rec. 12, 25.

Luffi, P., Ducea, M.N., 2022. Chemical mohometry: assessing crustal thickness of ancient orogens using geochemical and isotopic data. Rev. Geophys. 60. https://doi.org/10.1029/2021RG000753.

Lund, K., Box, S.E., Holm-Denoma, C.S., San Juan, C.A., Blakely, R.J., Saltus, R.W., Anderson, E.D., DeWitt, E., 2015. Basement Domain Map of the Conterminous. United States and Alaska. U.S. Geological Survey Data Series, Data Series, vol. 898, pp. 1–41.

Mahan, K.H., Allaz, J.M., Baird, G.B., Kelly, N.M., 2013. Proterozoic metamorphism and deformation in the northern Colorado Front Range. In: Abbott, L.D., Hancock, G.S. (Eds.), Classic Concepts and New Directions: Exploring 125 Years of GSA Discoveries in the Rocky Mountain Region. In: America Field Guide, vol. 33. Geological Society, pp. 185–204.

Marshall, E.W., Lassiter, J.C., Barnes, J.D., Luguet, A., Lissner, M., 2017. Mantle melt production during the 1.4 Ga Laurentian magmatic event: isotopic constraints from Colorado Plateau mantle xenoliths. Geology 45, 519–522. https://doi.org/10.1130/G38891.1.

McCoy, A.M., Karlstrom, K.E., Shaw, C.A., Williams, M.L., 2005. The Proterozoic ancestry of the Colorado Mineral Belt: 1.4 Ga shear zone system in Central Colorado. In: Karlstrom, K.E., Keller, G.R. (Eds.), The Rocky Mountain Region: An Evolving Lithosphere. In: Geophysical Monograph Series, pp. 71–90.

Mitchell, R.N., Zhang, N., Salminen, J., Liu, Y., Spencer, C.J., Steinberger, B., Murphy, J.B., Li, Z.X., 2021. The supercontinent cycle. Nat. Rev. Earth Environ. 2, 358–374. https://doi.org/10.1038/s43017-021-00160-0.

Mole, D.R., Kirkland, C.L., Fiorentini, M.L., Barnes, S.J., Cassidy, K.F., Isaac, C., Belousova, E.A., Hartnady, M., Thebaud, N., 2019. Time-space evolution of an Archean craton: a HF-isotope window into continent formation. Earth-Sci. Rev. 196, 102831. https://doi.org/10.1016/j.earscirev.2019.04.003.

Premo, W.R., Moscati, R.J., DeWitt, E., Gilmer, A.K., Hillenbrand, I.W., 2023. Data release of geochemical, geochronologic, and isotopic data for Precambrian to Cenozoic rocks from Colorado, New Mexico, Utah, and Wyoming. U.S. Geological Survey data release. https://doi.org/10.5066/P9ZD6DFW.

Profeta, L., Ducea, M.N., Chapman, J.B., Paterson, S.R., Gonzales, S.M.H., Kirsch, M., Petrescu, L., DeCelles, P.G., 2015. Quantifying crustal thickness over time in magmatic arcs. Sci. Rep. https://doi.org/10.1038/srep17786.

Roberts, N.M.W., Salminen, J., Johansson, Å., Mitchell, R.N., Palin, R.M., Condie, K.C., Spencer, C.J., 2022. On the enigmatic mid-Proterozoic: single-lid versus plate tectonics. Earth Planet. Sci. Lett. 594, 117749. https://doi.org/10.1016/j.epsl.2022.117749.

Shaw, C.A., Karlstrom, K.E., 1999. The Yavapai-Mazatzal crustal boundary in the Southern Rocky Mountains. Rocky Mt. Geol. 34, 37–52. https://doi.org/10.2113/34.1.37.

Shaw, C.A., Heizler, M.T., Karlstrom, K.E., 2005. 40Ar/39Ar thermochronologic record of 1.45–1.35 Ga intracontinental tectonism in the southern Rocky mountains: interplay of conductive and advective heating with intracontinental deformation. Geophys. Monogr. Ser. 154, 163–184. https://doi.org/10.1029/154GM12.

Sibson, R., 1981. A brief description of natural neighbor interpolation. In: Interpolating Multivariate Data. John Wiley & Sons, New York.

Sizova, E., Gerya, T., Brown, M., 2014. Contrasting styles of Phanerozoic and Precambrian continental collision. Gondwana Res. 25, 522–545. https://doi.org/10.1016/j.gr.2012.12.011.

Spear, F.S., 1993. Metamorphic Phase Equilibria and Pressure-Temperature-Time Paths. Mineralogical Society of America Monograph. Mineralogical Society of America, Washington, D.C.

Spencer, C.J., Mitchell, R.N., Brown, M., 2021. Enigmatic mid-Proterozoic orogens: hot, thin, and low. Geophys. Res. Lett. 48, 1–12. https://doi.org/10.1029/2021GL093312.

Stern, R.J., 2020. The mesoproterozoic single-lid tectonic episode: prelude to modern plate tectonics. GSA Today 30, 4–10. https://doi.org/10.1130/GSATG480A.1.

Tang, M., Xu, C., Jihua, H., Bing, S., 2021. Orogenic quiescence in Earth's middle age. Science 371, 728–731. https://doi.org/10.1126/science.abf1876.

Turner, S.J., Langmuir, C.H., 2015. The global chemical systematics of arc front stratovolcanoes: evaluating the role of crustal processes. Earth Planet. Sci. Lett. https://doi.org/10.1016/j.epsl.2015.03.056.

Van Schmus, W.R., Bickford, M.E., Turek, A., 1996. Proterozoic geology of the east-central Midcontinent basement. In: van der Pluijm, B.A., Catacosinos, P.A. (Eds.), Basement and Basins of Eastern North America. Geological Society of America, pp. 7–31.

Weller, O.M., Mottram, C.M., St-Onge, M.R., Möller, C., Strachan, R., Rivers, T., Copley, A., 2021. The metamorphic and magmatic record of collisional orogens. Nat. Rev. Earth Environ. 2, 781–799. https://doi.org/10.1038/s43017-021-00218-z.

Whitmeyer, S.J., Karlstrom, K.E., 2007. Tectonic model for the Proterozoic growth of North America. Geosphere 3, 220–259. https://doi.org/10.1130/GES00055.1.

Williams, M.L., Karlstrom, K.E., 1996. Looping P-T paths and high-T, low-P middle crustal metamorphism: Proterozoic evolution of the southwestern United States. Geology 24, 1119–1122. https://doi.org/10.1130/0091-7613(1996)024<1119:LPTPAH>2.3.CO;2.

Williams, M.L., Karlstrom, K.E., Lanzirotti, A., Read, A.S., Bishop, J.L., Lombardi, C.E., Pedrick, J.N., Winsted, M.B., 1999. New Mexico middle-crustal cross sections: 1.65-Ga macroscopic geometry, 1.4-Ga thermal structure, and continued problems in understanding crustal evolution. Rocky Mt. Geol. 34, 53–66. https://doi.org/10.2113/34.1.53.

Wooden, J.L., Miller, D.M., 1990. Chronologic and isotopic framework for Early Proterozoic crustal evolution in the eastern Mojave Desert Region, SE California. J. Geophys. Res., Solid Earth 95, 20133–20146. https://doi.org/10.1029/JB095iB12p20133.

Zhu, Z., Campbell, I.H., Allen, C.M., Brocks, J.J., Chen, B., 2022. The temporal distribution of Earth's supermountains and their potential link to the rise of atmospheric oxygen and biological evolution. Earth Planet. Sci. Lett. 580. https://doi.org/10.1016/j.epsl.2022.117391.